RESEARCH ARTICLE

WILEY ENERGY RESEARCH
INTERNATIONAL JOURNAL OF

Effective MgO-doped TiO$_2$ nanoaerogel coating for crystalline silicon solar cells improvement

Fanchao Meng[1] (iD) | Zahir Dehouche[1] | Aorrapum Nutasarin[1] | George R. Fern[2]

[1]Brunel University London, College of Engineering, Design and Physical Sciences, Uxbridge UB8 3PH, UK

[2]Brunel University London, Department of Chemical and Materials Engineering, Uxbridge UB8 3PH, UK

Correspondence
Fanchao Meng, College of Engineering, Design and Physical Sciences, Brunel University London, Uxbridge UB8 3PH, UK.
Email: fanchao.meng@brunel.ac.uk

Summary

This study looks at investigating the influence of high surface area TiO$_2$ and MgO-doped TiO$_2$ aerogel nanomaterials to improve the photovoltaic performance of monocrystalline silicon (mono-Si) solar cells. TiO$_2$ and MgO-doped TiO$_2$ anatase nanoaerogels were synthesized via a single-step colloidal homogeneous precipitation sol-gel method in a compact high-pressure hydrogen reactor. TiO$_2$-based nanoparticles were encapsulated in ethylene vinyl acetate resins, and the obtained composite solutions were screen printed on the textured surface of the cells. The specific surface area, microstructural, composition, and optical properties of the nanoaerogels were characterized by Brunaur-Emmett-Teller, X-ray powder diffractometer, energy-dispersive X-ray spectroscopy, field emission transmission electron microscope, field emission scanning electron microscope, and ultraviolet-visible spectrophotometry. We observed that the MgO-doped TiO$_2$ (2% mol) nanoaerogel exhibited a much superior specific surface area (231 m^2/g) compared with the undoped TiO$_2$ (154 m^2/g). Experimental results showed that the calculated relative power conversion efficiency increased by 4.6% for the MgO-doped TiO$_2$ coating and 3.4% for the undoped TiO$_2$ under a simulated one-sun illumination.

KEYWORDS

ethylene vinyl acetate, high-pressure hydrogen reactor, MgO-doped TiO$_2$ nanoaerogel, monocrystalline silicon (mono-Si) solar cells

1 | INTRODUCTION

Nowadays, the crystalline silicon (c-Si) solar cell is still the most technically mature and widely used photovoltaic (PV) device for direct generation of electricity from solar radiation owing to its abundance, stability, and nontoxicity. However, the high generation cost and relatively low efficiency are still the barriers to the development prospects of these systems at large scale.[1,2] The theoretical maximum energy conversion efficiency for a c-Si solar cell with bandgap energy (E_g) of 1.12 eV is limited to 30%,[3] primarily due to the blackbody radiation, radiative recombination, and spectral losses. Among these, the spectrum losses represent the highest loss in the silicon solar cell, including nonabsorbable photons with energy below the band gap ($h_v < E_g$) and the strong thermalization caused by above-bandgap photons.[4] To overcome the challenges mentioned above, the promotion of light absorption through the solar cell is required. This can be achieved by enhancing the effective photon path length and light trapping capability of the solar cell. Antireflective coating (ARC),[5] surface texturing,[6,7] and incorporation of nanotructured light harvesting materials[8-10] are widely used to improve the light trapping and minimize the recombination, thereby increasing the conversion efficiency of solar cell.

In recent years, titanium dioxide (TiO_2) has been extensively studied owing to its nontoxicity, chemical stability, and high photocatalytic activity.[11] Titanium dioxide (especially anatase phase) exhibits good reactivity under ultraviolet (UV) light and is currently employed as a cost-effective ARC in the domain of PV cells.[12,13] Furthermore, nanostructured TiO_2, such as nanotubes, nanofibers, nanoparticles, and nanocrystals, have been proven to provide superior photocatalytic performance due to their large surface area.[14-16] However, the wide bandgap of TiO_2 (3.2 eV for anatase and 3.0 eV for rutile) restricts the absorption to the UV region.[17] For this reason, a number of approaches have been devised, such as doping with metallic (eg, Fe, Cr, and Mg)[18-20] and non-metallic elements (eg, N and S)[21,22] into the TiO_2 lattice, which could effectively improve the photocatalytic activity of TiO_2 in both UV and visible regions. An alternative strategy is to obtain high surface area of TiO_2 particles with microporous or mesoporous structures because the porous texture on the TiO_2 NPs opens up the possibility for light diffusion on the interface of semiconductor and promotes rapidly the photogenerated-electron transfer to the conduction band of TiO_2 NPs. Moreover, the high surface area and porous structure allow multiple reflections of incident light and provide a good scattering effect, which enhances the light harvesting capability of TiO_2 across a wide wavelength.[23-25]

There are many reports about the effects of TiO_2-based NPs on the enhanced performance of PV devices,[23,25,26] but less research is now carried out on c-Si solar cells.[27,28] Herein, we report on the potential application of TiO_2 and magnesium oxide (MgO)-doped TiO_2 NPs to improve the conversion efficiency of commercial single junction mono-Si solar cells. In the present work, mesoporous TiO_2 and MgO-doped TiO_2 aerogels were prepared through an innovative approach by using a precipitation method in conjunction with a modified sol-gel process.[29] In addition, to encapsulate the TiO_2-based NPs on the textured surface of the solar cells without loss of UV activity, EVA was used as a binder.[30] Hence, we believe that such a combination of element doping method with the use of nanoporous photocatalyst could compensate for the low spectral response of silicon solar cells at the UV-blue wavelengths while improving light trapping.

This work demonstrated the formation of a novel anti-reflection layer comprising EVA/TiO_2-based nanocomposite on top of the mono-Si solar cell by using blade screen printing. In addition to the investigation of the microstructure of the nanocomposite layer, the PV current density-voltage (*J-V*) characteristics, optical reflectance, and external quantum efficiency (EQE) response of mono-Si solar cells before and after coating were also presented to examine the effectiveness of the TiO_2-based nanoaerogels.

2 | EXPERIMENTAL

2.1 | Materials

The chemicals in this work are all used as received without further purification. Methanol (99%) and p-xylene (99%) were purchased from Alfa Aesar Reagent Co, Ltd, UK. Titanium (IV) chloride (99.9%) and magnesium nitrate hexahydrate (99.999%) were purchased from Sigma Aldrich Reagent Co, LLC, UK.

2.2 | Synthesis of TiO_2-based aerogels

For preparation of nanostructured TiO_2-based nanoaerogels, titanium (IV) chloride ($TiCl_4$) and magnesium nitrate hexahydrate (Mg $(NO_3)_2 \cdot 6H_2O$) were used as the precursor of TiO_2 and MgO dopant. In a typical synthetic process, 1.4 mL of $TiCl_4$ was gently injected into a glass beaker containing 150 mL of methanol and 63.6 mg of Mg $(NO_3)_2 \cdot 6H_2O$ salt to obtain a 1/50 molar ratio of magnesium to titanium in the synthesized NPs. This molar ratio is suggested by a study in which different molar ratios of MgO-doped TiO_2 NPs were prepared by an aerogel method, and it was found that a solid solution of MgO-TiO_2 mixed oxides of 1:50 ratio exhibited the optimum performance in UV-active photocatalysis.[20] The mixture of that solution was vigorously stirred for 15 minutes where $TiCl_4$ is fully dissolved in methanol at room temperature. The contents were then poured into an autoclave (Parr Model 5500) high-pressure compact stirred reactor, and H_2 gas was introduced into the autoclave at a pressure of 20 bar (2 MPa). The autoclave was then heated to a setting temperature of 200°C and maintained for 2 hours. The internal pressure was finally observed at around 80 bar (8 MPa). The autoclave was cooled down to room temperature, and the remaining H_2 gas was released. The autoclave was disassembled and the solution poured into a glass beaker. The solid aerogel obtained was washed 2 times with methanol and dried in a fume hood overnight at room temperature. The synthesized powder was finally calcined in a furnace at 400°C for 10 hours under a static air environment. The synthetic process for undoped TiO_2 aerogel is similar with that of MgO-doped TiO_2. The only difference between those 2 cases is the adding of Mg dopant.

2.3 | Formation of the deposited layer

The solar cells used in this work are commercial mono-Si PV cells (XS156B3-200R, Motech Industry, Taiwan) flanked with dark silicon nitride (SiN_x) antireflection coatings. The SiN_x layer (thickness ≈ 80 nm) was deposited by plasma-enhanced chemical vapor deposition. For

experimental purposes, the cell was cut into 3 equal sizes (156 mm × 52 mm) by using a high-power laser (TMX90, CTR, UK).

(1) EVA layer

The EVA copolymer (Dupont, France) was used as encapsulant for TiO_2 NPs to the solar cell. To determine the best weight ratio (wt%) of EVA to TiO_2-based NPs that contributes to an optimum enhancement of power conversion efficiency (PCE) in the PV cells, various weight ratios of EVA/p-xylene liquid mixtures (9, 12, 15, 18, and 21 wt%) were previously prepared by dissolving stoichiometric amounts of EVA foils in p-xylene.

(2) Composite layer preparation

The synthesized undoped TiO_2 and MgO-doped TiO_2 NPs were ready to be used in the process of layer application. Prior to that process, 1.5 mg of each powder was measured and then dispersed in p-xylene by using an ultrasonic bath. The solution with different concentrations of dispersed powder (0.2, 0.3, 0.4, 0.6, and 0.8 mg/mL) are prepared and then separately mixed with certain amounts of EVA sheet. The mixture solution was then left above 30°C under magnetic stirring until uniform colloidal solutions were observed.

(3) Layer Application

The as-prepared mixture solution was then blade screen printed on the SiN_x antireflection layer of the solar cells, with a coated area of 25 (5 cm × 5 cm) cm^2. The coated cells were then cured in a furnace at 190°C for 5 minutes. After the heat treatment, the applied mixture of EVA/MgO-TiO_2 formed a glossy layer on the textured surface of the solar cell. In addition, the solar cells with solely EVA coatings were also produced for comparison. An illustration of the steps for preparation of MgO-doped TiO_2 NPs and their integration on the surface of mono-Si solar cell is presented in Figure 1.

2.4 | Characterization

The electrical characteristics of the solar cells were performed on the uncoated and coated parts of each cell (illuminated area = 8.04 cm^2) by using a solar simulator (OAI Trisol TSS156, USA) under one-sun illumination (1000 W/m^2) and room temperature conditions. (The spectral mismatch error was estimated to be at 0.9%.) In these particular experiments, the source meter (Keithley 2601B, USA) was employed to obtain *J-V* curves, with sweeping parameters of voltage over the range from −1 to 1 V through 50 data points with 50-ms interval time for each reading. (The rated error in the short-circuit current on the tested cell was less than 0.03%.) The curing temperature of EVA was determined by using a single-furnace differential scanning calorimeter (PerkinElmer DSC 6000, USA) with a built-in cooling accessory IntraCooler II refrigerator. During the measurement, 12 mg of EVA foil was enclosed in an aluminum sample pan and heated from −20 to 220°C at 10°C/min for 2 cycles while testing the heat flow.

The reflectance, transmission, and absorption spectra were measured by using an UV-visible spectrophotometer (Perkin Elmer Lambda 650S, USA). External quantum
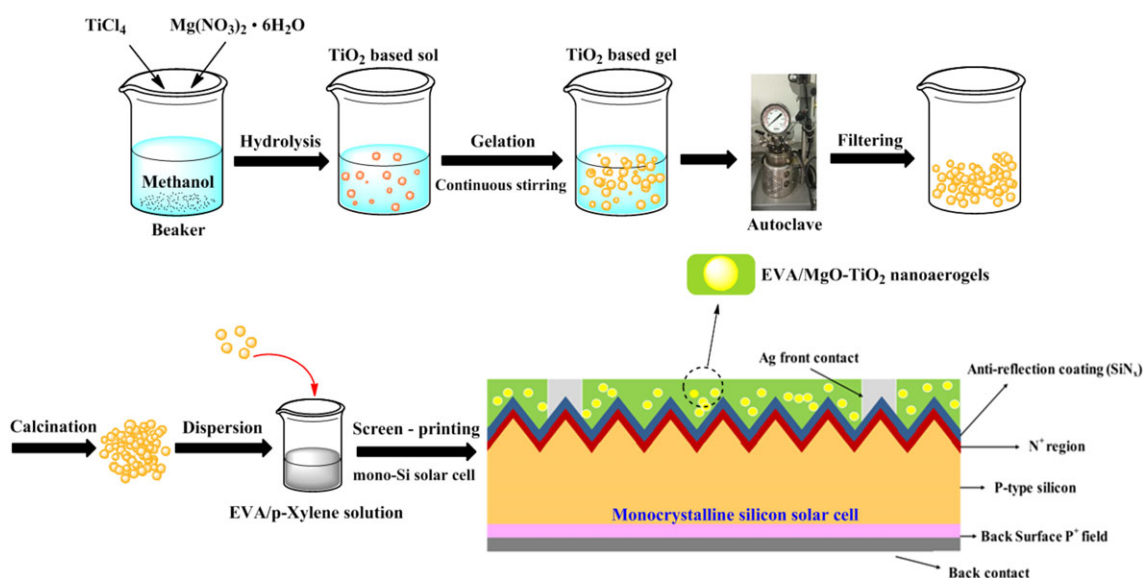

FIGURE 1 Flow diagram showing the fabrication process of TiO_2-based nanoaerogels and their integration onto the surface of mono-Si solar cell [Colour figure can be viewed at wileyonlinelibrary.com]

efficiency measurements were carried out by using a monochromator-based solar cell spectral response system (EQE-PVE300, Bentham, UK). The specific surface area and pore diameter of synthesized TiO_2-based aerogels were measured by nitrogen gas physisorption at 77.4 K (−196.15°C) by using surface area and pore size analyzer (NOVAtouch LX1, USA). The surface area is obtained by using the Brunaur-Emmett-Teller equation to a relative pressure (P/P_0) range of 0.1 to 0.3 of the adsorption isotherm. The pore diameter is determined from the adsorption branch of isotherm by applying density functional theory. The surface morphology was obtained with a field emission scanning electron microscope (FE-SEM; SUPRA 35 VP, ZEISS, Germany). Energy-dispersive X-ray spectroscopy is used for elemental analysis of the deposited layers. The structural features and particle sizes were examined by an FE transmission electron microscope (FE-TEM; JEM-2100F, JEOL, USA). The crystalline phases of the synthesized powders were identified by using a Bruker D8 Advance X-ray powder diffractometer with CuKα (λ = 0.154 nm) radiation over the 2θ range of 5 to 100°. The diffractometer was previously calibrated by using an aluminum oxide line position standard from Bruker and LaB_6 NIST SRM 660a line profile shape standard.

3 | RESULTS AND DISCUSSION

3.1 | Differential scanning calorimetry measurement

Differential scanning calorimeter thermodynamic measurement was used to determine the curing temperature that enhances the transparency of the EVA raw material. It can be seen from Figure 2 that the first heating curve shows an endothermic peak at 48.75°C with an enthalpy
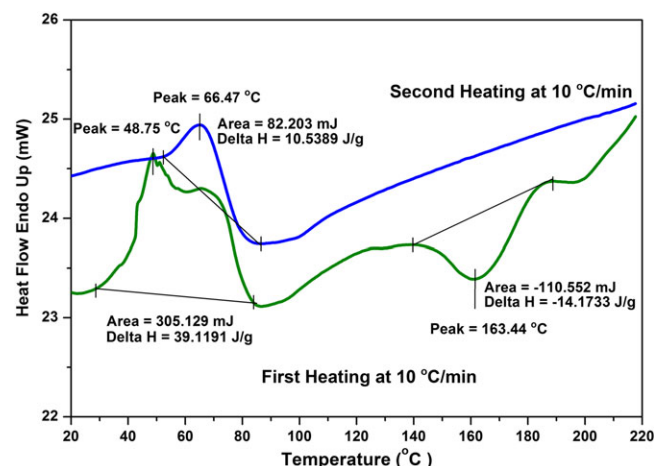
of 39.12 J/g. The exothermic peak occurred at 163.44°C with the curing enthalpy of 14.17 J/g. The second heating curve shows a lower melting peak of 10.54 J/g compared with the first scan (39.12 J/g), and no exothermic peak can be detected, implying full curing of EVA. The shift in the endothermic peak, the reduction of the melting enthalpy, and the disappearance of the curing peak suggest a change in the EVA's crystal structure.[31] From the first heating curve, we have observed that the exothermic region is completed at 186°C, which represents the optimum curing temperature for the coated solar cell.

3.2 | X-ray powder diffraction

Figure 3 depicts the X-ray diffraction (XRD) patterns of the MgO-doped TiO_2 and undoped TiO_2 powders annealed at 400°C. The first peak of each diffraction pattern indicates the most stable plane of TiO_2 (2θ = 25.30°, d_{101} = 3.5174 Å) and MgO-doped TiO_2 (2θ = 25.25°, d_{101} = 3.5239 Å), respectively, which are in good agreement with the standard card of the anatase TiO_2 phase (JCPDS 84-1286, 2θ = 25.32°, d_{101} = 3.5141 Å). However, the XRD patterns of MgO-TiO_2 (1:50 M) did not show the presence of MgO as the quantity of added dopant is too low to form an independent crystalline phase of MgO and the Mg^{2+} ions could disperse into the TiO_2 lattice. The line broadening of MgO-doped TiO_2 XRD patterns indicates a slight structural change, suggesting a reduction in the crystallite size. To determine the average size (τXRD) of the NPs, we used Scherrer equation[32]:

$$\tau = \frac{K\lambda}{\beta\cos\theta} \tag{1}$$

FIGURE 2 The differential scanning calorimetry heating curves of raw ethylene vinyl acetate material [Colour figure can be viewed at wileyonlinelibrary.com]
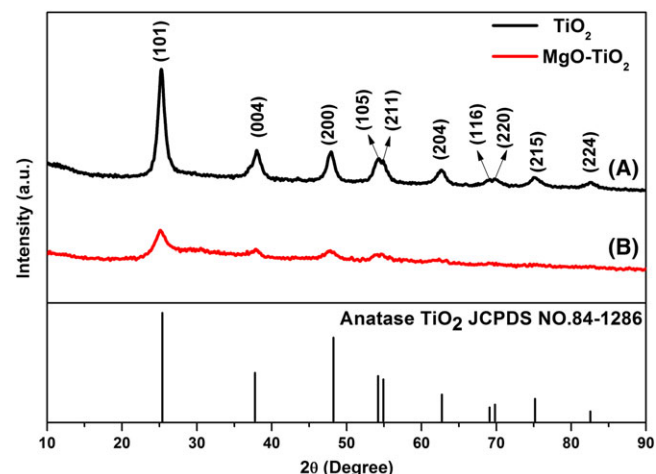

FIGURE 3 X-ray powder diffractometer patterns of (A) TiO_2 and (B) MgO-doped TiO_2 nanoparticles annealed at 400°C for 10 hours [Colour figure can be viewed at wileyonlinelibrary.com]

where λ is the wavelength of the incident X-rays (1.5406 Å), β is the full width at half maximum in radian, θ is the diffraction angle of the considered diffraction line, and K is the Scherrer constant (0.89). The results show comparable crystallite sizes of ~9.2 and ~7.1 nm for TiO_2 and MgO-doped TiO_2, respectively.

3.3 | Morphology analysis

Figure 4A to C shows the FE-SEM micrographs of MgO-doped TiO_2 nanoaerogels. The agglomeration of the particles with roughly spherical shape can be clearly observed. The cross-section image (see Figure 4D) of a coated cell indicates good dispersion of agglomerated NPs. It shows also the pyramidally textured silicon surface and the deposited EVA/MgO-doped TiO_2 composite layer with an average thickness of 9 μm.

The high-resolution FE-TEM image (see Figure 5D) of dispersed NPs indicates their crystalline nature with lamellar lattice morphology. However, the statistical analysis of the size distribution from TEM data was difficult to obtain due to the agglomeration of the NPs. The size ranges of 5 to 15 nm were measured from those discrete particles. The energy-dispersive X-ray spectroscopy (see Figure 6) from the entire FE-SEM scanned area of coated cells confirms the presence of Ti, O, and Mg elements in the deposited layers. The additional peaks corresponding to C are from the EVA binder. The insignificant intensity peaks of Fe and Cr observed in the spectra are most likely due to the contamination during the fabrication process when the reaction solution is being stirred at high temperature-pressure in the stainless steel autoclave.

3.4 | Structural properties of synthesized TiO_2-based aerogels

Figure 7A and B shows the nitrogen-sorption isotherms of TiO_2 and MgO-doped TiO_2 aerogels prepared in current work. The TiO_2 aerogels show a specific surface area of ~154.3 m^2/g, which is comparable with the aerogels (82 m^2/g) prepared by using high-temperature supercritical drying of sol-gel methods, as reported by Koodali et al.[29] The density functional theory pore size distribution plot (see Figure 7C) indicates a typical mesoporosity ranging from 4 to 20 nm[33] with pores centered at 6.8 nm. In MgO-doped TiO_2 aerogels, the pore size distribution plot (see Figure 7D) exhibits a sharp peak, indicating comparatively smaller pores centered at 5.2 nm, and a larger surface area of ~231.4 m^2/g was observed. The remarkable increase of surface area in MgO-doped TiO_2 nanoaerogels is attributed to the slight reduction in grain size, which is mainly caused by the interface stress and lattice contraction resulting
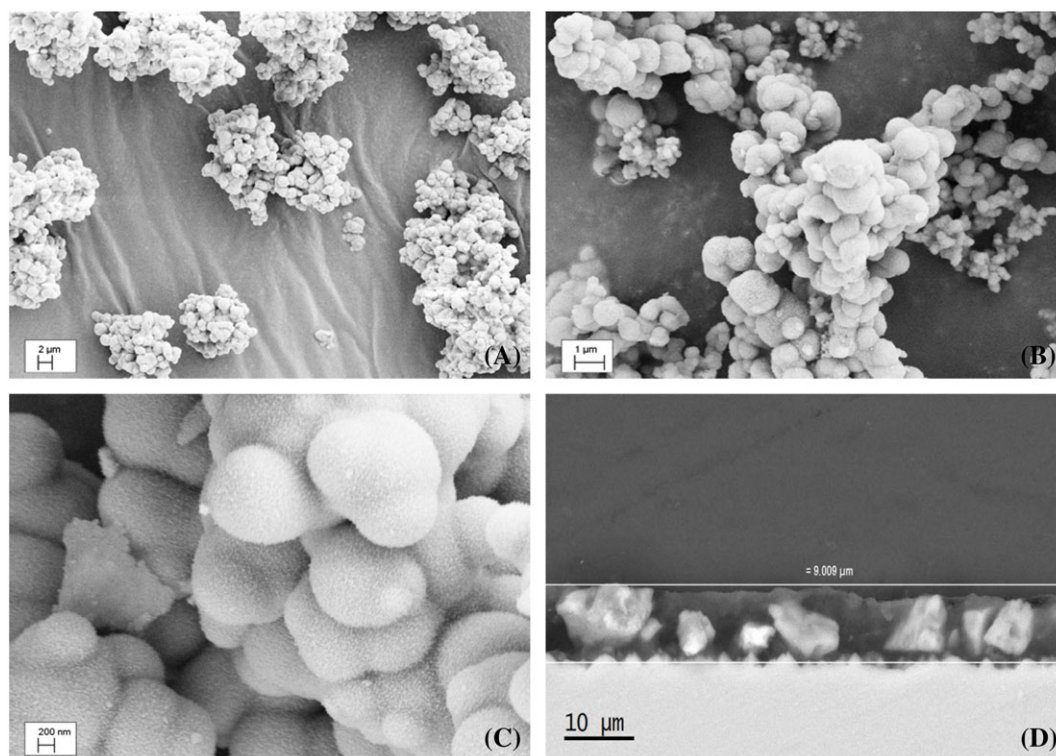

FIGURE 4 Field emission scanning electron microscope micrographs of (A-C) MgO-doped TiO_2 nanoaerogels annealed at 400°C and (D) cross-section image of solar cell after coating with ethylene vinyl acetate/MgO-doped TiO_2 [Colour figure can be viewed at wileyonlinelibrary.com]
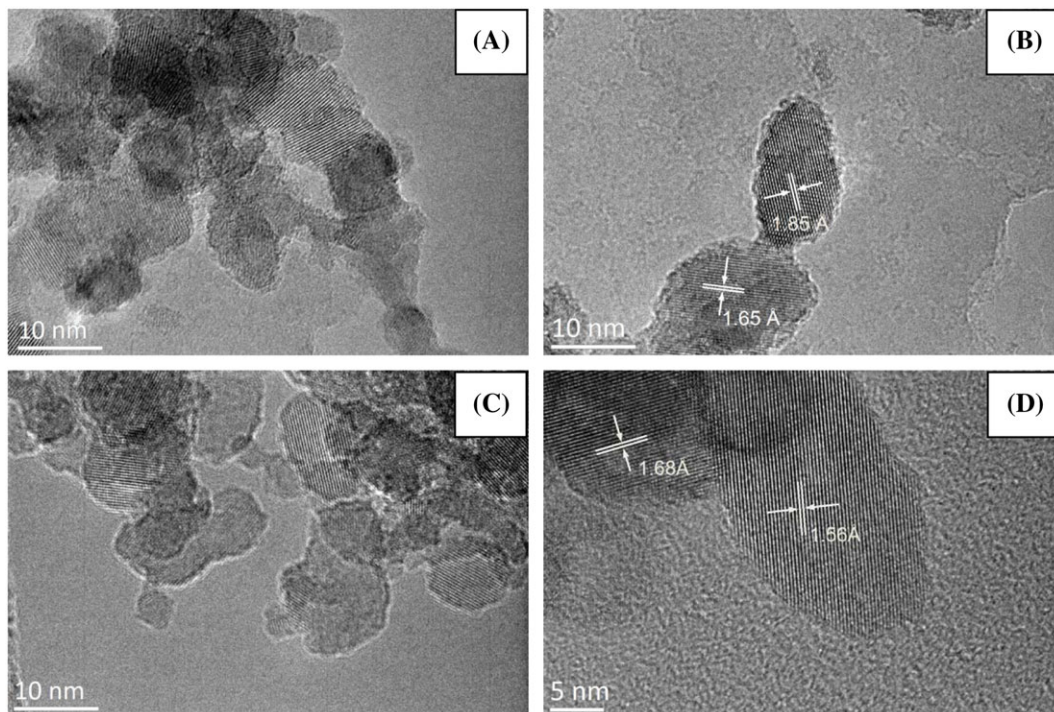
FIGURE 5 A to C, Field emission transmission electron microscope micrographs of TiO_2. D, MgO-doped TiO_2 nanoaerogel annealed at 400°C [Colour figure can be viewed at wileyonlinelibrary.com]
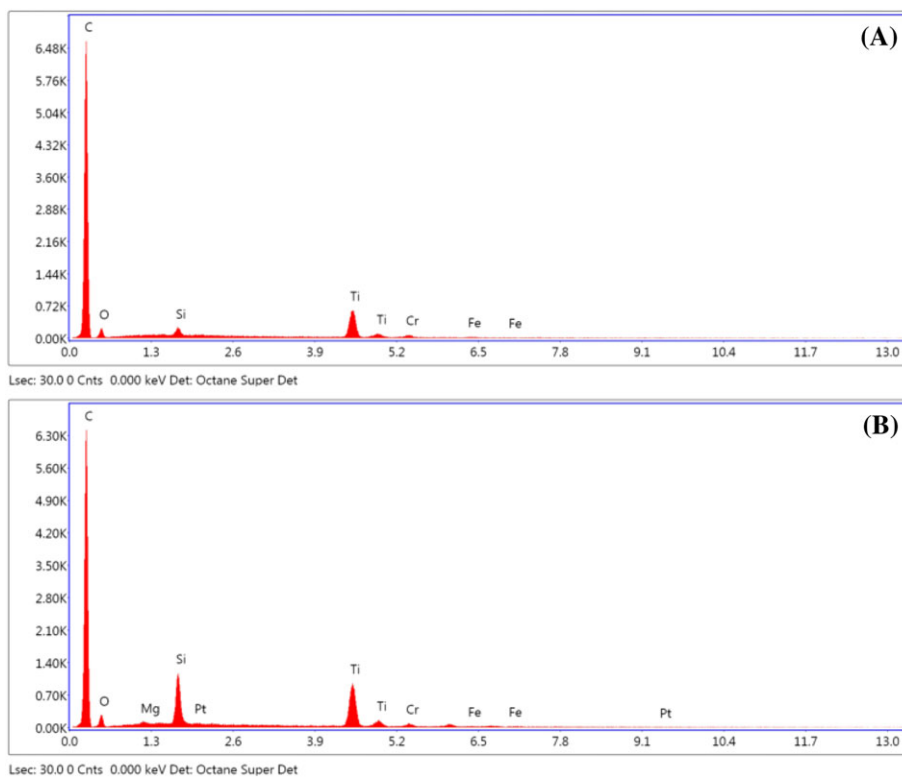

FIGURE 6 Energy-dispersive X-ray spectroscopy of mono-Si solar cells coated with (A) ethylene vinyl acetate (EVA)/TiO_2 and (B) EVA/MgO-doped TiO_2 [Colour figure can be viewed at wileyonlinelibrary.com]
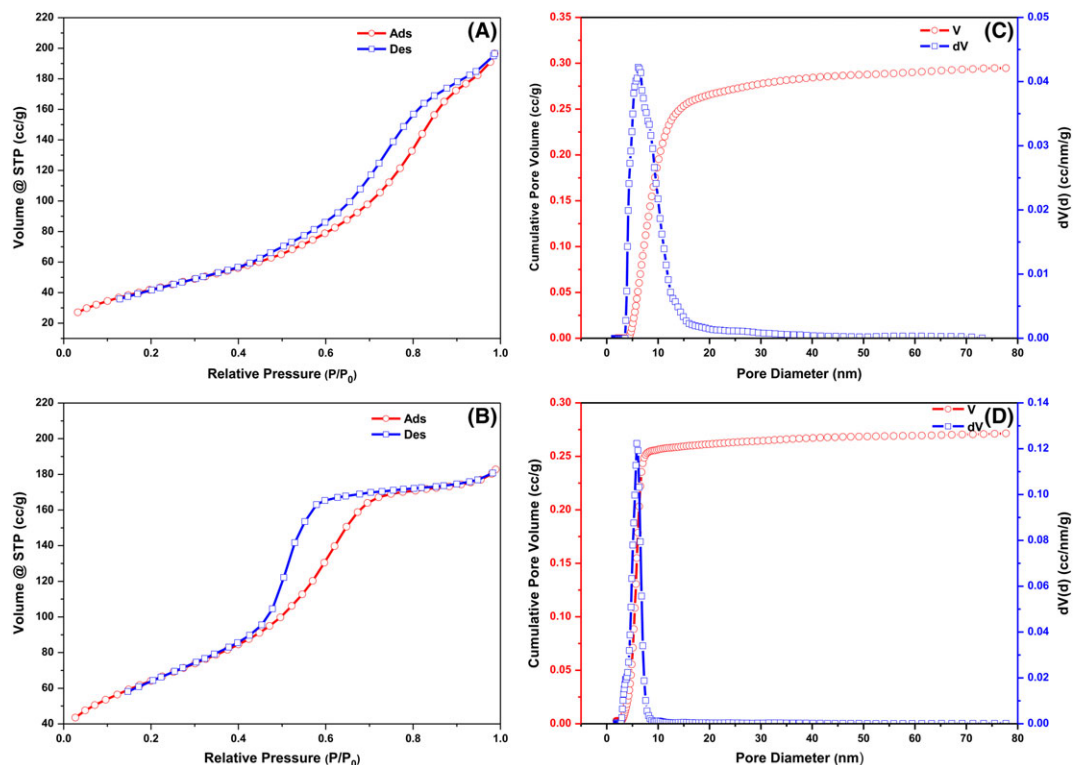
FIGURE 7 N_2-sorption isotherms of (A) representative TiO_2 aerogel and (B) MgO-doped TiO_2 aerogel; C and D, the corresponding pore size distribution plots are shown [Colour figure can be viewed at wileyonlinelibrary.com]

from the replacement of Ti (Ti^{4+} ionic radius = 0.057 nm) by Mg (Mg^{2+} ionic radius = 0.066 nm).[34] The detailed structural properties of the aerogels are summarized in Table 1.

3.5 | Coated solar cell characterization

The J-V characteristics of bare, solely EVA binder-coated, EVA/TiO_2, and EVA/MgO-TiO_2-coated solar cells are shown in Figure 8. The bare mono-Si solar cell exhibited a PCE of 18.19%, a short-circuit current density (J_{sc}) of 46.06 mA/cm^2, and an open-circuit voltage (V_{oc}) of 553.0 mV. After coating with 15 wt% EVA on the textured surface, the J-V characteristics showed a slight change in J_{sc} (45.81 mA/cm^2) and V_{oc} (553.1 mV). The formation of the EVA layer on top of the solar cells resulted in a marginal reduction of 0.08% (from 18.19% to 18.08%) in conversion efficiency. This coating provides the best electrical performance compared with other ratios of solely

EVA coatings, which can be seen from Table 2. In the case of the cell that was coated with EVA/TiO_2 nanocomposite at 0.3-mg/mL concentration, the J-V characteristics exhibited significant increase with ΔJ_{sc} = 0.76 mA/cm^2 and ΔV_{oc} = 6.8 mV, corresponding to an overall enhancement of 3.4% (from 18.19% to 18.81%) in PCE relative to those for a bare cell. The highest increase of ΔJ_{sc} = 1.43 mA/cm^2, corresponding to a maximum enhancement of 4.6% (from 18.19% to 19.03%), was achieved by integrating EVA/MgO-doped TiO_2 nanocomposite (0.3 mg/mL) on the cell's textured surface. The detailed characteristics of coated cells with TiO_2-based NPs at different concentrations are summarized in Table 3.

Figure 9 shows the enhancement in PCE of the coated cells as a function of deposited TiO_2-based NPs. It can be seen that the cells coated with MgO-doped TiO_2 NPs increased the conversion efficiency at all tested concentrations. The only reduction in PCE occurs in the cell

TABLE 1 Structural properties of TiO_2-based nanoaerogels

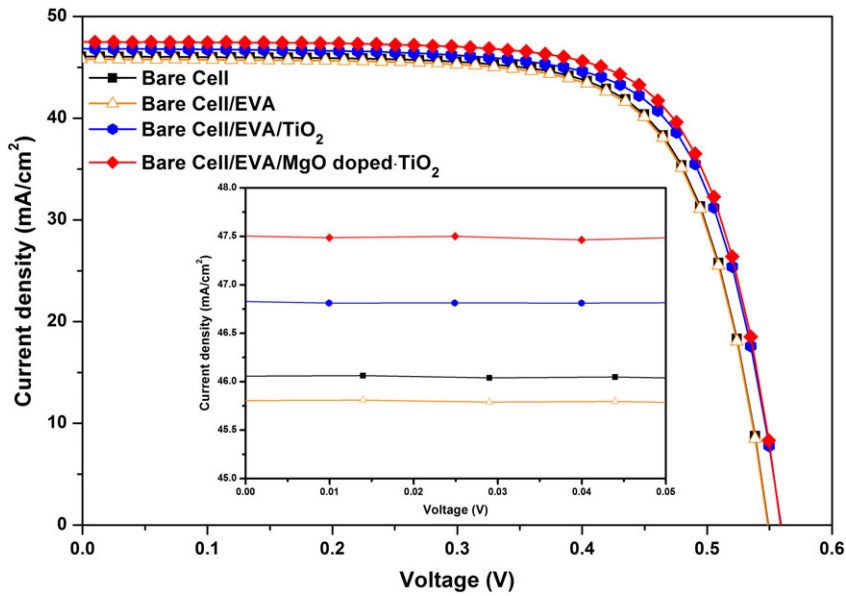| Materials	S_{BET} (m^2/g)	Pore Volume (cm^3/g)	Pore Diameter (nm)	Crystallite Size (nm)
TiO_2 (this work)	154	0.29	6.8	9
MgO-doped TiO_2 (this work)	231	0.27	5.2	7
TiO_2[29]	82	0.25	11	20

FIGURE 8 Photovoltaic *J-V* curves of mono-Si solar cells before and after coating with solely ethylene vinyl acetate (EVA), EVA/TiO₂, and EVA/MgO-doped TiO₂ [Colour figure can be viewed at wileyonlinelibrary.com]

TABLE 2 Power conversion efficiency change in mono-Si solar cell coated with different wt% ratios of ethylene vinyl acetate (EVA)

Cell Type	Concentration in wt%	Uncoated η (%)	Coated η (%)	Change in Absolute η (%)
EVA	9	18.23	17.77	−0.46
EVA	12	18.12	17.84	−0.28
EVA	15	18.19	18.08	−0.08
EVA	18	18.19	18.01	−0.18
EVA	21	18.22	18.01	−0.21

TABLE 3 *J-V* characteristics of mono-Si solar cells before and after coating with solely EVA, EVA/TiO₂, and EVA/MgO doped-TiO₂

Cell Type	J_{sc} (mA/cm²)	V_{oc} (mV)	P_{max} (W)	FF	PCE (%)
Uncoated	46.06	553.0	0.1463	0.714	18.19
Cell/EVA	45.81	553.1	0.1454	0.714	18.08
Cell/EVA/TiO₂ (0.2 mg/mL)	46.29	558.1	0.1497	0.719	18.62
Cell/EVA/TiO₂ (0.3 mg/mL)	46.82	559.8	0.1513	0.718	18.81
Cell/EVA/TiO₂ (0.4 mg/mL)	46.06	556.3	0.1474	0.716	18.34
Cell/EVA/TiO₂ (0.6 mg/mL)	46.16	553.6	0.1467	0.714	18.25
Cell/EVA/TiO₂ (0.8 mg/mL)	45.92	551.4	0.1452	0.713	18.06
Cell/EVA/MgO-TiO₂ (0.2 mg/mL)	46.53	558.4	0.1506	0.719	18.73
Cell/EVA/MgO-TiO₂ (0.3 mg/mL)	47.49	561.0	0.1530	0.722	19.03
Cell/EVA/MgO-TiO₂ (0.4 mg/mL)	46.89	558.7	0.1523	0.721	18.94
Cell/EVA/MgO-TiO₂ (0.6 mg/mL)	46.64	557.3	0.1499	0.717	18.65
Cell/EVA/MgO-TiO₂ (0.8 mg/mL)	46.03	553.5	0.1467	0.715	18.24

EVA, ethylene vinyl acetate; FF, fill factor; PCE, power conversion efficiency.

coated with undoped TiO₂ NPs at 0.8 mg/mL (18.19% to 18.06%), which we think is due to the aggregation of particles that diminishes the light-trapping capability of the cell's intrinsic textured surface, which can cause excessive backward scattering.[35]

3.6 | Optical characteristics of coated solar cell

Figures 10 and 11 show the optical reflectance and absorption spectra measured from uncoated, solely
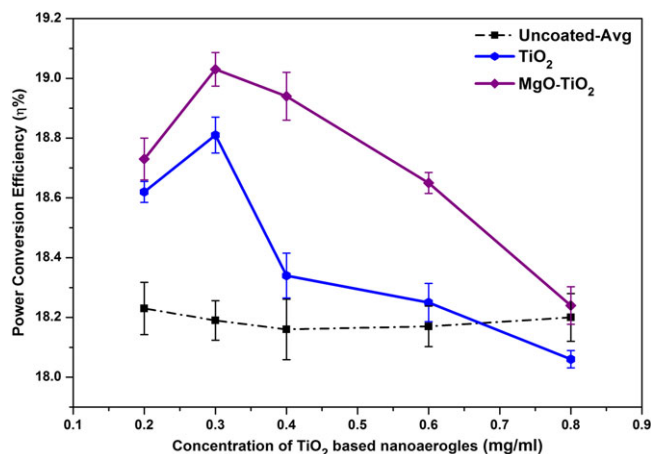
FIGURE 9 Enhancement in power conversion efficiency of mono-Si solar cells coated with ethylene vinyl acetate (EVA)/TiO$_2$ and EVA/MgO-doped TiO$_2$ with the concentration of dispersed nanoparticles [Colour figure can be viewed at wileyonlinelibrary.com]
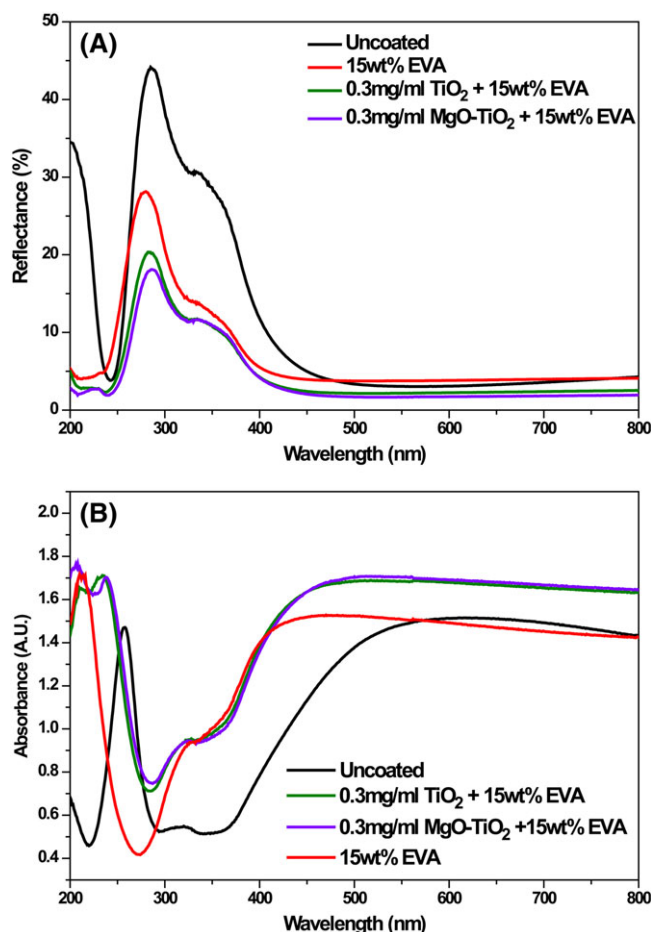

FIGURE 10 Optical (A) reflectance and (B) absorbance of uncoated and coated cells [Colour figure can be viewed at wileyonlinelibrary.com]

EVA-coated, EVA/TiO$_2$-coated, and EVA/MgO-TiO$_2$-coated solar cells. It could be seen that coated cells with enhanced electrical characteristics exhibit overall less reflectance and higher absorbance compared with uncoated cells across the measured spectral wavelength range from 200 to 800 nm. The reflectance of coated cell with EVA/MgO-TiO$_2$ shows a more significant reduction at wavelengths of 250 to 400 nm. Furthermore, the comparison also indicates that the reflectance in the spectrum range from 300 to 450 nm can be reduced when the cell's surface is coated with EVA, which basically coincides with our predictions because the average refractive index of EVA ($n \approx 1.48$) is between the SiN$_x$ antireflection coating layer ($n \approx 1.9$) and air ($n \approx 1$).[30,36] As indicated, the EVA serves as a binder for the TiO$_2$-based NPs. These layers tend to decrease the cells' efficiency. It is pivotal to find a certain wt% of EVA that decreases efficiency by a fairly small amount or even provides some minor enhancement. Actually, we observed that the solely 15 wt% EVA coating possesses good light transparency with transmittance close to that of a glass substrate (see Figure 12). Moreover, the coated substrate with EVA/MgO-doped TiO$_2$ shows slightly higher transmittance as compared with the EVA/undoped-TiO$_2$.

The reduced reflectance for the enhanced solar cells is achieved by the light scattering from the spherical TiO$_2$-based nanoaerogels, as a result of improving in overall light trapping at the interface of the textured ARC layer. Because the light scattering abilities rely largely upon the particle size, the larger particles may cause an increased cross section for backward scattering, which shades the pyramid structures.[35] In this work, the diameter of the TiO$_2$-based nanoaerogels (5-15 nm) was much less than the spacing between the pyramids. Hence, the particles did not impair the light benefits on the original ARC layer, whereas the incident light was forward scattered into the cell through the TiO$_2$-based NPs. Furthermore, the aerogels with mesoporous microstructure potentially allow more incident light to transmit through the pore and shine onto the ARC layer over a large angular range, increasing the optical path length of photons in the cell, thereby enhancing the light harvesting.[23,25] The drastic reduction of reflectance in the range of 250 to 350 nm is due to the absorption of high-energy incident photons mainly in the short-middle wavelength UV region. This can be confirmed by the UV-visible absorption spectra (see Figure 11) in which the absorption by MgO-TiO$_2$ mixed oxides (MgO:TiO$_2$ = 1:50) was observed at the shorter wavelength. The calculated results show good approximation of optical energy band gaps of 3.10 and 3.17 eV for the deposited EVA/TiO$_2$ and EVA/MgO-TiO$_2$, respectively.

The surface modification of the mixed oxide by adding small amounts of MgO into TiO$_2$ nanoaerogels is a more reasonable explanation for the additional reduced reflectance. When Mg^{2+} ions are doped into the TiO$_2$
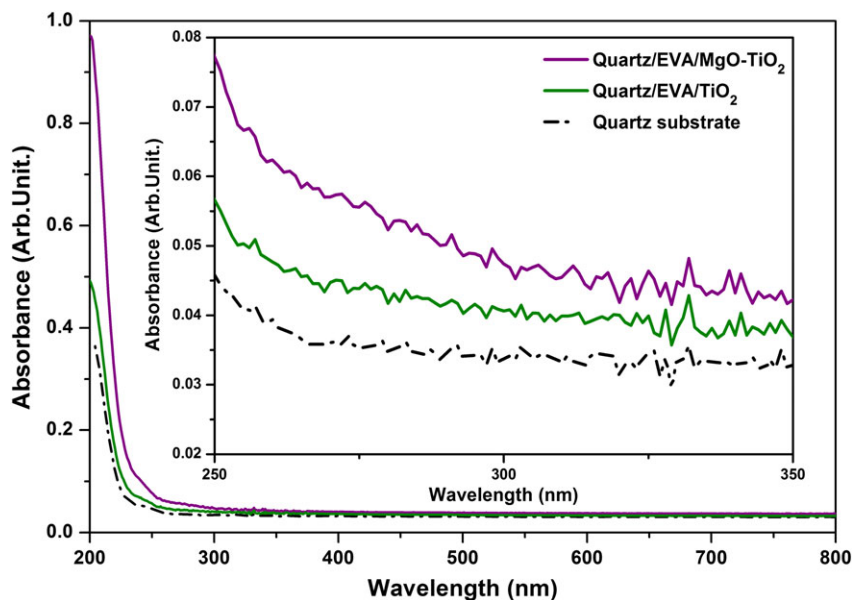
FIGURE 11 Ultraviolet-visible absorption spectra of quartz substrate and the deposited nanocomposite films of ethylene vinyl acetate (EVA)/TiO$_2$ and EVA/MgO-doped TiO$_2$ [Colour figure can be viewed at wileyonlinelibrary.com]
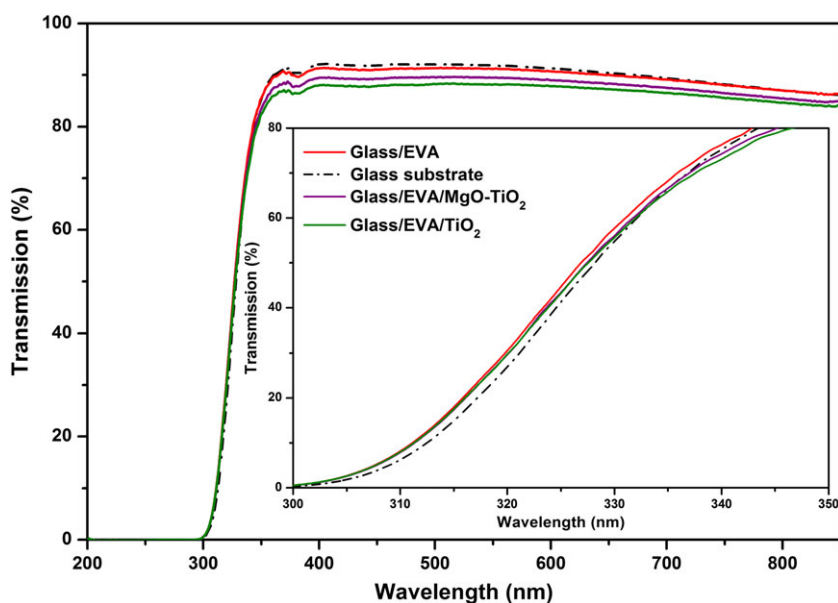

FIGURE 12 Transmission spectra for glass substrate and the deposited composite films with the following configurations: glass with solely ethylene vinyl acetate (EVA), glass with EVA/TiO$_2$, and glass with EVA/MgO-doped TiO$_2$ [Colour figure can be viewed at wileyonlinelibrary.com]

nanoaerogels, various types of crystal defects and vacancies are created to compensate the charge neutrality in TiO$_2$ crystal, contributing to further enhancement in the UV photocatalytic reactivity.[20,37,38] In addition, the smaller NPs with higher surface-to-volume ratio may probably induce more photons to be absorbed at the short-middle wavelength UV region for photo-current conversion.[23,25]

3.7 | External quantum efficiency characterization

Figure 13A presents the EQE response for bare, solely EVA binder-coated, EVA/TiO$_2$-coated, and EVA/MgO-TiO$_2$-coated solar cells. The EQE value for binder-coated cells is fairly close to that of bare cells and is slightly higher at wavelengths of 300 to 330 nm, which achieves a close match with the reflectance measurements (see Figure 10A). Furthermore, the solar cells coated with EVA/TiO$_2$ and EVA/MgO-TiO$_2$ composite layers provide enhanced photocurrent across the entire wavelength range from 300 to 1100 nm and more significant increase in EQE in the UV-region compared with the bare cell. This is due to the improved anti-reflective properties of EVA/TiO$_2$ and SiN$_x$, giving rise to an overall increase of photon harvesting on the cell's textured surface. Compared with the EVA/TiO$_2$ coated cell, the solar cell with EVA/MgO-TiO$_2$ layer achieves a more pronounced increase in EQE, particularly at wavelengths of 300 to 350 nm. These findings are also consistent with those
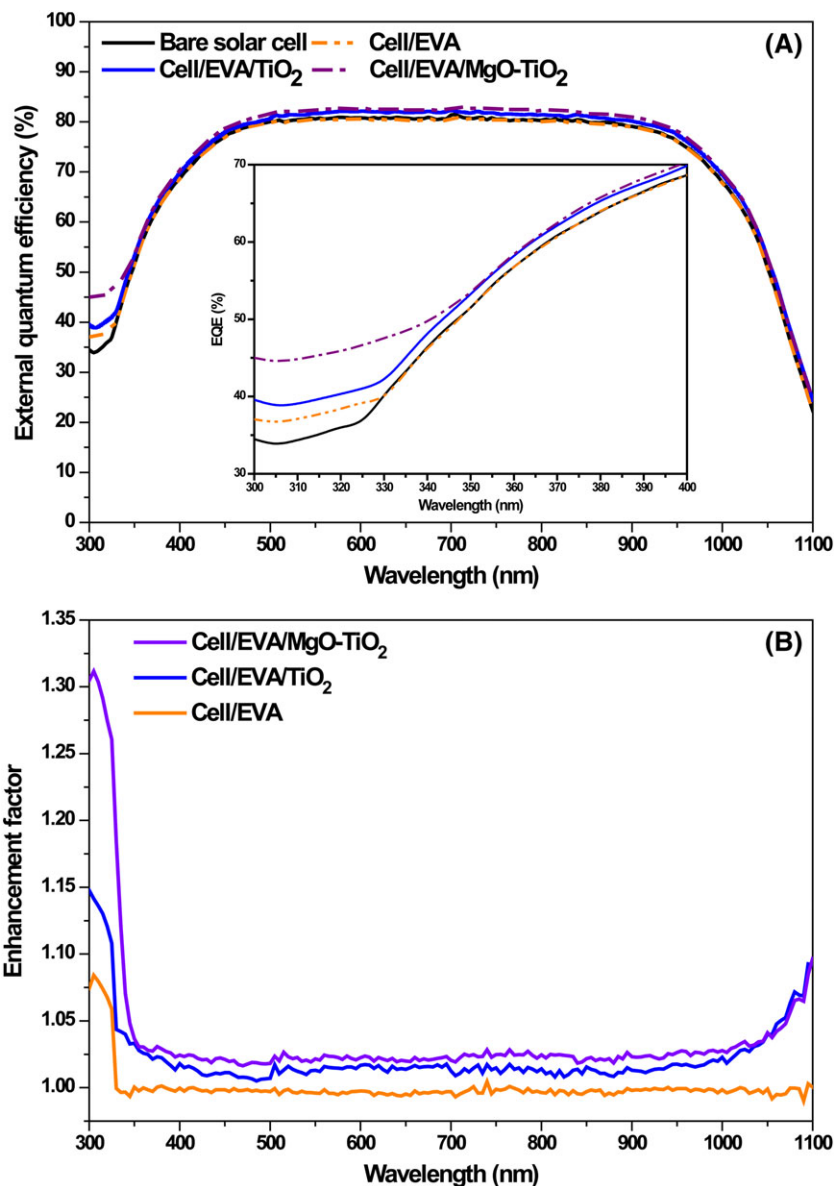
FIGURE 13 A, External quantum efficiency (EQE) curves of all cells evaluated in this study; B, enhancement factor of EQE for cell coated with solely ethylene vinyl acetate (EVA), EVA/TiO$_2$, and EVA/MgO-doped TiO$_2$, compared that of bare cell [Colour figure can be viewed at wileyonlinelibrary.com]

observed variations in reflectance and J_{sc}. Figure 13B plots the enhancement factor of EQE for all cells evaluated in this work. The cells coated with EVA/MgO-TiO$_2$ obtained the maximal EQE enhancement factor (˃1, 300-1100 nm) followed by the cells coated with EVA/TiO$_2$.

4 | CONCLUSION

In this paper, we reported the successful synthesis of high surface area nanostructured TiO$_2$-based aerogels and developed a novel ARC for mono-Si solar cells by screen printing a solution of TiO$_2$-based NPs dispersed in an EVA matrix onto the textured surface of solar cells. Experimental results revealed that the as-prepared MgO-TiO$_2$ aerogels with low content of MgO (2 mol%) have a

higher surface area (231 m^2/g) compared with that of undoped TiO$_2$ aerogels (154 m^2/g), and their application to the textured surface of solar cells led to significant improvements in EQE and J_{sc}. This enhancement was attributed to the conjunction effects of improved antireflective properties of TiO$_2$-based NPs and EVA binder. Nanoporous TiO$_2$ could enhance the light scattering capability and increase the photon harvesting on the pyramidal structures. The binder with 15 wt% ratio provides good optical and mechanical host conditions for the TiO$_2$-based NPs. Ethylene vinyl acetate encapsulated TiO$_2$ NPs enhance electrical performance, but not as much as MgO-doped TiO$_2$. An optimum relative enhancement of 4.6% was observed in a cell with MgO-doped TiO$_2$ nanocomposite at particle density of 0.3 (mg/mL).

ORCID

Fanchao Meng 🔟 http://orcid.org/0000-0003-1338-8035

REFERENCES

1. Battaglia C, Cuevas A, Wolf SD. High-efficiency crystalline silicon solar cell: status and perspectives. *Energ Environ Sci.* 2016;9(5):1552-1576.

2. Green MA, Hishikawa Y, Dunlop ED, Levi DH, Hohl-Ebinger J, Ho-Baillie AWY. Solar cell efficiency tables (version 51). *Prog Photovolt Res Appl.* 2018;26(1):3-12.

3. Shockley W, Queisser HJ. Detailed balance limit of efficiency of p-n junction solar cells. *J Appl Phys.* 1961;32(3):510-519.

4. Green MA. *Third Generation Photovoltaic: Advanced Solar Energy Conversion.* Germany: Springer, Berlin & Heidelberg; 2003.

5. Kang MH, Ryu K, Upadhyaya A, Rohatgi A. Optimization of SiN AR coating for Si solar cells and modules through quantitative assessment of optical and efficiency loss mechanism. *Prog Photovolt Res Appl.* 2011;19(8):983-990.

6. Kim J, Inns D, Fogel K, Sadana DK. Surface texturing of single-crystalline silicon solar cells using low density SiO_2 films as an anisotropic etch mask. *Sol Energy Mater Sol Cells.* 2010;94(12):2091-2093.

7. Höhn O, Tucher N, Bläsi B. Theoretical study of pyramid sizes and scattering effects in silicon photovoltaic module stacks. *Opt Express.* 2018;26(6):A320-A330.

8. Baryshnikova KV, Petrov MI, Babicheva VE, Belov PA. Plasmonic and silicon spherical nanoparticle antireflective coatings. *Sci Rep.* 2016;6:1-11.

9. Raj B, Voorde MVD, Mahajan Y. *Nanotechnology for Energy Sustainability.* New York: John Wiley & Sons; 2017 137 p.

10. Yu R, Lin QF, Leung SF, Fan ZY. Nanomaterials and nanostructures for efficient light absorption and photovoltaics. *Nano Energy.* 2012;1(1):57-72.

11. Nakata K, Fujishima A. TiO_2 photocatalysis: design and application. *J Photochem Photobiol C.* 2012;13(3):169-189.

12. Richards BS. Single-material TiO_2 double-layer antireflection coatings. *Sol Energy Mater Sol Cells.* 2003;79(3):369-390.

13. Arabatzis I, Todorova N, Fasaki I, et al. Photocatalytic, self-cleaning, antireflective coating for photovoltaic panels: characterization and monitoring in real conditions. *Sol Energy.* 2018;159:251-259.

14. Addamo M, Bellardita M, Paola AD, Palmisano L. Preparation and photoactivity of nanostructured anatase, rutile and brookite TiO_2 thin films. *Chem Commun.* 2006;0(47):4943-4945.

15. Sajan CP, Wageh S, Al-Ghamdi AA, Yu JG, Cao SW. TiO_2 nanosheets with exposed {001} facets for photocatalytic applications. *Nano Res.* 2016;9(1):3-27.

16. Jin Z, Meng FL, Jia Y, et al. Porous TiO_2 nanowires derived from nanotubes: synthesis, characterization and their enhanced photocatalytic properties. *Microporous Mesoporous Mater.* 2013;181:146-153.

17. Cheng J, Wang YT, Xing Y, Shahid M, Pan W. A stable and highly efficient visible-light photocatalyst of TiO_2 and heterogeneous carbon core-shell nanofibers. *RSC Adv.* 2017;7(25):15330-15336.

18. Moradi H, Eshaghi A, Hosseini SR, Ghani K. Fabrication of Fe-doped TiO_2 nanoparticles and investigation of photocatalytic decolorization of reactive red 198 under visible light irradiation. *Ultrason Sonochem.* 2016;32:314-319.

19. Hajjaji A, Trabelsi K, Atyaoui A, et al. Photocatalytic activity of Cr-doped TiO_2 nanoparticles deposited on porous multicrystalline silicon films. *Nanoscale Res Lett.* 2014;9(543):1-6.

20. Shrestha KM, Sorensen CM, Klabunde KJ. MgO-TiO_2 mixed oxide nanoparticles: comparison of flame synthesis versus aerogel method; characterization, and photocatalytic activities. *J Mater Res.* 2013;28(3):431-439.

21. Cheng XW, Yu XJ, Xing ZP, Yang LS. Synthesis and characterization of N-doped TiO_2 and its enhanced visible-light photovoltaic activity. *Arab J Chem.* 2016;9:S1706-S1711.

22. Zhu MS, Zhai CY, Qiu LQ, et al. New method to synthesize S-doped TiO_2 with stable and high efficient photocatalytic performance under indoor sunlight irradiation. *ACS Sustainable Chem Eng.* 2015;3(12):3123-3129.

23. Singh N, Salam Z, Subasri A, Sivasankar N, Subramania A. Development of porous TiO_2 nanofibers by solvosonication process for high performance quantum dot sensitized solar cell. *Sol Energy Mater Sol Cells.* 2018;179:417-426.

24. Ming H, Ma Z, Huang H, et al. Nanoporous TiO_2 spheres with narrow pore size distribution and improved visible light photocatalytic abilities. *Chem Commun.* 2011;47(28):8025-8027.

25. Al-Attafi K, Nattestad A, Yamauchi Y, Dou SX, Kim JH. Aggregated mesoporous nanoparticles for high surface area light scattering layer TiO_2 photoanodes in dye-sensitized solar cells. *Sci Rep.* 2017;7(10341):1-8.

26. Su PY, Fu WY, Yao HZ, et al. Enhanced photovoltaic properties of perovskite solar cells by TiO_2 homogeneous hybrid structure. *R Soc Open Sci.* 2017;4(10):1-6.

27. Gad KM, Vössing D, Richter A, et al. Ultrathin titanium dioxide nanolayers by atomic layer deposition for surface passivation of crystalline silicon. *IEEE J Photovolt.* 2016;6(3):649-653.

28. Yang XB, Bi QY, Ali H, Davis K, Schoenfeld WV, Weber K. High-performance TiO_2-based electron-selective contacts for crystalline silicon solar cells. *Adv Mater.* 2016;28(28):5891-5897.

29. Parayil SK, Psota RJ, Koodali RT. Modulating the textural properties and photocatalytic hydrogen production activity of TiO_2

by high temperature supercritical drying. *Int J Hydrogen Energy.* 2013;38(25):10215-10225.

30. French RH, Rodríguez-Parada JM, Yang MK, Derryberry RA, Pfeiffenberger NT. Optical properties of polymeric materials for concentrator photovoltaic systems. *Sol Energy Mater Sol Cells.* 2011;95(8):2077-2086.

31. Stark W, Jaunich M, Bohmeyer W, Lange K. Investigation of the crosslinking behaviour of ethylene vinyl acetate (EVA) for solar cell encapsulation by rheology and ultrasound. *Polym Test.* 2012;31(7):904-908.

32. Cullity BD. *Elements of X-Ray Diffraction*. Reading, Massachusetts: Addison-Wesley Publishing Company, Inc; 1956, 262 p.

33. Thommes M, Kaneko K, Neimark AV, et al. Physisorption of gases, with special reference to the evaluation of surface area and pore size distribution (IUPAC technical report). *Pure Appl Chem.* 2015;87:1051-1069.

34. Qin W, Nagase T, Umaskoshi Y, Szpunar JA. Lattice distortion and its effects on physical properties of nanostructured materials. *J Phys Condens Matter.* 2007;19(23):1-8.

35. Tishkovets VP, Petrova EV, Jockers K. Optical properties of aggregate particles comparable in size to the wavelength. *J Quant Spectrosc Radiat Transf.* 2004;86(3):241-265.

36. Wei MC, Chang SJ, Tsia CY, Liu CH, Chen SC. SiN_x deposited by in-line PECVD for multi-crystalline silicon solar cells. *Sol Energy.* 2006;80(2):215-219.

37. Anpo M, Yamada Y, Kubokawa Y. Photoluminescence and photocatalytic activity of MgO powders with co-ordinatively unsaturated surface ions. *J Chem Soc Chem Commun.* 1986;0(9):714-716.

38. Pacchioni G, Ferrari AM. Surface reactivity of MgO oxygen vacancies. *Catal Today.* 1999;50(3-4):533-540.